J. Coat. Technol. Res., **12** (4) 767–776, 2015
DOI 10.1007/s11998-015-9676-1

Preparation of tough silicon-oxo coatings with enhanced hardness from moisture-curable polysiloxane and silica alcosol

Ting He, Shuxue Zhou

Abstract Hardness and toughness are typically contradictive for sol–gel-derived coatings. In this article, thick (~15 μm) silicon-oxo-dominated nanocomposite coatings with high transparency were fabricated by incorporating 3-methacryloxypropyltrimethoxysilane (MPS)-modified silica alcosol into a moisture-curable polysiloxane oligomer and curing with the aid of 3-aminopropyltriehtoxysilane (APS). Effects of MPS-to-SiO_2 molar ratio, SiO_2 nanoparticle content, APS dosage, and curing process on the mechanical properties were thoroughly investigated using a pencil hardness tester, a flexibility tester, and a nanoindentation tester. The best properties were achieved by a coating with an MPS-to-SiO_2 molar ratio of 0.1:1, a silica nanoparticle content of 10 wt%, and an APS dosage of 30 wt%. This coating demonstrated enhanced hardness (pencil hardness = 7H and microhardness = 626 MPa) and toughness (excellent flexibility of 5 mm in the mandrel bend test). Additional curing via aza-Michael addition between amino groups from APS and C=C groups from the polysiloxane oligomer can be accomplished at elevated temperatures. This enables further mechanical enhancement, namely hardness (9H and 1087 MPa), with adequate flexibility (10 mm). Such properties are superior to those reported for other sol–gel-derived silicon-oxo coatings produced at low drying temperatures.

Keywords Polysiloxane, Colloidal silica, Sol–gel, Nanocomposite coatings, Mechanical properties

T. He, S. Zhou (✉)
Department of Materials Science and State Key Laboratory of Molecular Engineering of Polymers, Advanced Coatings Research Center of Ministry of Education of China, Fudan University, Shanghai 200433, China
e-mail: zhoushuxue@fudan.edu.cn

Introduction

Sol–gel-derived coatings attract much interest because they show promise as scratch-resistant coatings,[1] anti-corrosion coatings,[2] and optical coatings.[3] Among them, silicon-oxo-dominated coatings are the most common due to the versatility of silicon-oxo sources; low cost; and high stability in light, heat, water, and organic solvents. Their mechanical properties and wettability can be readily adjusted by the number and types of organic groups bonded to the silicon-oxo backbone. These advantages provide multifarious opportunities to attain high performance coatings.

Sol–gel-derived silicon-oxo coatings are usually synthesized by hydrolysis/condensation of alkoxysilanes followed by drying at various temperatures. Those alkoxysilanes include tetraalkoxysilane [$Si(OR)_4$], organotrialkoxysilane [$X\text{-}Si(OR)_3$], and organodialkoxylsilane [$XY\text{-}Si(OR)_2$], in which the organic groups (X,Y) are methyl, phenyl, vinyl, glydyloxypropyl, methacryloxypropyl, and aminopropyl, among others. Silicon-oxo coating curing takes place via condensation reactions between Si-OH groups or between an Si-OH group and an Si-OR group. Additionally, some bonded organic groups can react to aid or even dominate the curing, for example, epoxy/amine reactions[4] and radical polymerization of methacrylic moieties.[5] Generally, a high number of alkoxyl groups, rigid organic groups, and high curing temperatures result in hard and brittle silicon-oxo coatings with thicknesses limited to <10 μm, and sometimes <1 μm because of cracking. Sol–gel-derived silica coatings[6] and Ormocer coatings[7] are two typical coating examples that have been developed since the mid-1980s. Although coating brittleness can be alleviated by reducing the degree of condensation of the silicon-oxo-backbone, and/or by increasing the flexibility of the side organic group, coating strength is always simultaneously reduced. In the most extreme case, polydimethylsiloxane coatings can possess excellent

flexibility, but show low hardness and strength. The hardness and toughness of silicon-oxo coatings seem to contradict one another.[8] Thus, preparing hard and tough silicon-oxo coatings with a sol–gel process is a great challenge.

Besides the precursor and curing process, prohydrolysis of alkoxysilanes,[9,10] the curing agent,[11] and additional nanofillers (such as colloidal silica[12] and AlOOH[13]) may also remarkably influence the mechanical properties of sol–gel-derived silicon-oxo coatings. These variables complicate the process of fabricating coatings with optimized mechanical properties, but provide potential for achieving hard and tough silicon-oxo coatings, and have rarely been reported to date.

In our previous study,[9] we successfully prepared hard, tough, thick polysiloxane coatings by prehydrolysis of methacryloxypropylmethyldimethoxysilane (MPDS) and methyltriethoxysilane (MTES), followed by moisture curing in the presence of aminopropyltriethoxysilane (APS). Further incorporation of methacryloxypropyltrimethoxysilane (MPS)-modified tungsten-doped vanadium dioxide [VO_2(W)] increased the microhardness from 473 to 990 MPa, but did not sacrifice the flexibility.[14] Inspired by this result, MPS-modified colloidal silica was employed as a nanofiller in moisture-curable polysiloxane coatings to understand whether mechanically reinforced silicon-oxo coatings can be fabricated using these inexpensive nanoparticles. Thorough investigations were conducted to determine the effects of MPS:silica molar ratio, colloidal silica content, APS dosage, and curing process on the mechanical properties of the coatings. A hard (1.09 GPa, 9H) and tough (flexibility = 10 mm) silicon-oxo coating with thickness up to 15 μm was obtained. To our knowledge, these mechanical properties are superior and rarely reported for sol–gel-derived silicon-oxo coatings prepared at low temperature (≤ 185°C). The reinforcement mechanism is also discussed in this study.

Experimental

Materials

MPDS (98%), MTES (98%), MPS (98%), and APS (98%) were purchased from Zhangjiagang Guotaihuarong New Chemical Materials Co., Ltd. of China. Silica alcosol (30% solid content, particle size = 20 nm) was purchased from Zhangjiagang Churen New Materials Co., Ltd. of China. Aqueous ammonia solution (25 wt%) and absolute ethanol (AR) were purchased from Sinopharm Chemical Reagent Co., Ltd.

Synthesis of polysiloxane oligomer

The polysiloxane oligomer was synthesized according to a previously reported method.[9] MPDS 5.81 g (0.05 mol) and MTES 40.12 g (0.45 mol) were added to a 100-mL round-bottom flask and magnetically stirred. Then, a diluted aqueous ammonia solution (4.5 g, concentration = 0.1 M) and ethanol (5 g) were mixed and dropped into the flask over 15 min at room temperature. Afterward, the reaction mixture was heated to ~90°C in an oil bath and held for 4 h to obtain the polysiloxane oligomer.

Preparation of MPS-functionalized colloidal silica

Silica alcosol was added to a 50-mL round-bottom flask and magnetically stirred, and MPS was added dropwise to the stirring vessel. The reaction was carried out for 24 h at ambient temperature. The MPS-to-SiO_2 molar ratios were set as 0.05:1, 0.1:1, and 0.28:1, and the resulting modified silica alcosols were named S05, S10, and S28, respectively.

Fabrication of silicon-oxo-dominated coatings

The MPS-modified silica alcosol was mixed with the as-obtained polysiloxane oligomer solution and sonicated for approximately 3 min. APS was added to the solution in amounts of 10, 20, 30, and 50 wt% based on the mass of the as-obtained polysiloxane oligomer solution. Subsequently, each coating was cast on a tinplate by a drawdown rod (wet thickness = 120 μm), and cured in ambient conditions for 7 days, followed by further heat treatment at 60°C for 12 h. Unless otherwise noted, all coatings were dried with the above curing process. All tinplate sheets were polished with No. 0 (120 #) aluminum oxide cloth (Shanghai Grinding Wheel Works, China) and cleaned with acetone prior to casting. Coating formulations and their sample names are given in Table 1.

Characterization

Transmission electron microscopy (TEM) images were taken on a Hitachi H-800 TEM (Japan) at 75 kV to observe the dispersion of unmodified and MPS-modified silica particles in the coatings. Samples were prepared by drop-casting dilute solutions on copper grids and drying at room temperature.

Fourier transform infrared (FTIR) spectra were recorded using a Nicolet Nexus 470 FTIR spectrometer (USA) over the wavenumber ranging from 4000 to 400 cm^{-1} with a resolution of 4 cm^{-1} and accumulation of 32 scans. The unmodified SiO_2 and MPS-modified SiO_2 nanoparticles were separated from suspension in ethanol by centrifugation, washed three times with ethanol to remove residual MPS, and dried at 75°C for 2 h. The dried silica powders were blended with KBr to form sample pellets. The dried coatings were scraped from the substrate and then blended with KBr for FTIR analysis. The Raman spectra of the coatings

Table 1: The formulations and sample names of silicon-oxo nanocomposite coatings

Sample name	Silica alcosol		Colloidal silica content (%)[a]	Si-O content in dried coatings (%)[b]
	Type	Dosage (g)		
R0	–	0	0	40
R0-5	Unmodified	0.5	5	–
R0-10	Unmodified	1.0	10	–
R0-15	Unmodified	1.5	15	–
R0-20	Unmodified	2.0	20	–
R05-5	S05	0.5	5	41
R05-10	S05	1.0	10	45
R05-15	S05	1.5	15	46
R05-20	S05	2.0	20	–
R10-5	S10	0.5	5	44
R10-10	S10	1.0	10	48
R10-15	S10	1.5	15	49
R10-20	S10	2.0	20	–
R28-5	S28	0.5	5	45
R28-10	S28	1.0	10	48
R28-15	S28	1.5	15	50
R28-20	S28	2.0	20	–

In all formulations, 3 g of the as-obtained polysiloxane oligomer solution and 0.9 g of APS were used

[a] Mass percentages of silica nanoparticles based on the mass of the as-obtained polysiloxane oligomer solution

[b] As determined by TGA analysis from room temperature to 800°C

were recorded by a LABRAM-EB Raman spectroscope (Dilor Instrument, France). Coatings on tinplates were directly used for Raman characterization. An optical microscope (Hirox, Japan) was employed to determine coating thickness.

Pencil hardness was determined using MITSUBISHI UNI pencils with hardnesses varying from H to 9H according to the National Standard Testing Method (GB/T6739-1996) of China. The grade of the hardest pencil that did not cause surface lacerations was taken to be the pencil hardness. The flexibility was determined by a QTX paint flexibility tester (Shanghai Modern Environmental Engineering Technology Co., Ltd.) according to the National Standard Testing Method (GB/T1731-1993) of China. The tester has mandrel bars with diameters of 15, 10, 5, 4, 3, 2, and 1 mm, and the coating panel was bent around the mandrel bar. The smallest bar diameter that did not cause cracking in the coatings denotes the flexibility of the coatings. Higher mandrel diameters correspond to less flexible coatings.

Nanoindentation tests were conducted on a CSM nanoindentation instrument (CSM Instruments, Switzerland) using a Berkovich diamond indenter. The indenter contacts the surface first and then penetrates into the coatings at a constant strain rate of 0.05 s^{-1} until a depth of 1 μm is reached. The indenter holds at the maximum load for 50 s, and then withdraws from the surface at the same rate as loading. A minimum of five indentations were made for each sample. Hardness and elastic modulus were calculated from the loading-hold-unloading curves according to the Oliver and Pharr method.[15]

Nanoscratch tests were performed by a nanoscratch tester (CSM Instruments, Switzerland) using a Rockwell indenter (Rockwell-SB-B12, tip radius 10 μm, conical). After a prescan procedure with a minimum load of 1 mN, the tip was pressed into the samples with increasing load from 1 to 30 mN and moved at a constant rate of 4 μm/s. The surface profile was recorded by a depth sensor. A post-scan was performed at a load of 1 mN to determine the residual depth of the scratch. Meanwhile, an optical microscope was used to observe the scratch grooves. Three parallel scratches were applied for each sample, and the average value is reported.

Results and discussion

Preparation of silicon-oxo-dominated nanocomposite coatings

Preliminary experiments showed that direct addition of silica alcosol to the as-obtained polysiloxane oligomer solution resulted in an opaque mixture. Even after the addition of APS, the appearance of the coating did not change. This phenomenon suggests that the colloidal silica nanoparticles are not compatible with the moisture-curable polysiloxane. However, when a small quantity of MPS (MPS-to-SiO_2 molar ratio 0.05:1) was first added to silica alcosol, the silica alcosol/

polysiloxane oligomer solution did not make opaque coatings even at silica nanoparticle concentrations up to 20 wt%. Figure 1 presents the TEM images of the silicon-oxo coatings prepared with unmodified silica alcosol and modified silica alcosol (S05). Aggregates of silica nanoparticles are observed with unmodified silica alcosol, while all silica nanoparticles are individually dispersed in the coating fabricated with S05. These microscopic morphologies are in agreement with their macroscopic appearances.

The colloidal silica nanoparticles were centrifuged from the MPS-modified silica alcosol for FTIR characterization, as shown in Fig. 2. For comparison, the FTIR spectrum of the unmodified silica nanoparticles from original silica alcosol is also given in Fig. 2. Strong absorption peaks at 2957 and 1721 cm^{-1}, corresponding to the stretching vibrations of C–H and C=O, are revealed for the modified silica alcosols. This result indicates that MPS molecules are chemically bonded to silica nanoparticles in the MPS-modified silica alcosol. Therefore, improved compatibility between polysiloxane and modified silica alcosol may result from the methacrylic moieties that they both have. Figure 2 also shows that the intensity of the C=O peak increases with increasing molar ratio of MPS to SiO_2. This signifies that larger quantities of MPS are grafted on the surface of silica nanoparticles at higher MPS dosages.

The silicon-oxo-dominated coatings were highly stable in a sealed container. Once cast on substrates, they cured in ambient conditions and typically became tack-free within 2 h. The curing mechanism is expected to be related to the moisture-induced hydrolysis/condensation of Si-OH/Si-OR groups that exist in the moisture-curable polysiloxane resin. In addition, crosslinking reactions took place via aza-Michael addition between amino groups (from APS) and C=C groups (from tethered methacrylic moieties of polysiloxane oligomer), as demonstrated in our previous report.[9] Since methacrylic groups also exist on the surfaces of the colloidal silica nanoparticles, the silica nanoparticles may participate in film formation via aza-Michael addition during drying. Therefore, the curing mechanism is complicated in these silicon-oxo-dominated nanocomposite coatings.

The macro-mechanical properties of the silicon-oxo coatings

Pencil hardness and flexibility of silicon-oxo coatings are summarized in Table 2. Surprisingly, 5 wt% of unmodified silica nanoparticles induce a reduction in pencil hardness from 4H to H. Even though the R0-5 coating is soft, the flexibility is not better than that of the R0 coating. The mechanical deterioration may be attributed to poor interfacial interactions between the polysiloxane matrix and unmodified silica nanoparticles, as demonstrated above by aggregation of silica nanoparticles. As the content of unmodified silica nanoparticles increases further, the pencil hardness increases due to reinforcement by the silica nanoparticles, and flexibility declines. This mechanical behavior is analogous to behaviors exhibited in colloidal-silica-embedded organic coatings.[16] Thus, the

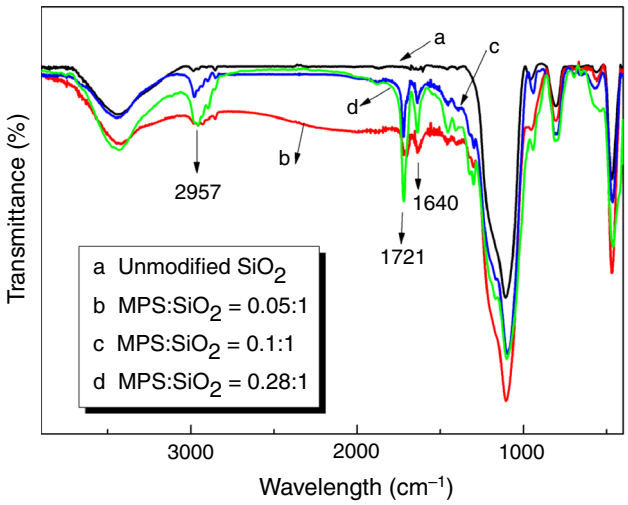

Fig. 2: FTIR spectra of unmodified and MPS-modified silica nanoparticles

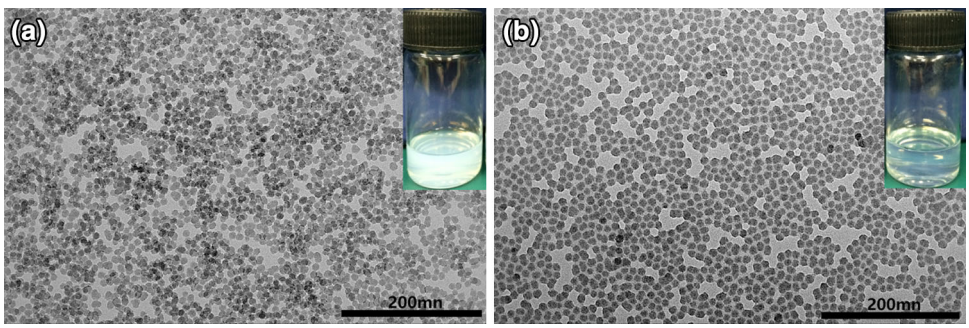

Fig. 1: TEM images of silicon-oxo coatings with (a) unmodified silica alcosol and (b) MPS-modified silica alcosol (S05). The insets are photographs of the corresponding coatings

Table 2: The macro-mechanical properties of silicon-oxo coatings

Sample	Thickness (μm)	Pencil hardness	Flexibility (mm)
R0	14.1	4H	10
R0-5	15.3	H	10
R0-10	14.5	3H	15
R0-15	14.9	5H	15
R0-20	14.1	5H	15
R05-5	16.2	4H	10
R05-10	16.1	3H	15
R05-15	16.7	6H	15
R05-20	17.1	5H	15
R10-5	14.1	4H	4
R10-10	14.9	7H	5
R10-15	16.6	6H	10
R10-20	15.5	5H	10
R28-5	16.2	3H	5
R28-10	15.9	4H	10
R28-15	17.6	4H	15
R28-20	17.8	5H	15
R10-10-10%[a]	14.7	H	4
R10-10-20%[a]	14.4	2H	5
R10-10-50%[a]	15.1	4H	10

[a] 10%, 20%, and 50% denote the APS dosage in the coatings based on the mass of the as-obtained polysiloxane oligomer solution. The APS dosage in all other samples is 30%

incorporation of unmodified silica alcosol is not an efficient route to produce hard and tough coatings.

The macro-mechanical properties evolve in a complicated way for coatings containing MPS-modified silica nanoparticles. The R05-X series of coatings (except the R05-5 coating) demonstrate similar mechanical properties to the R0-X coatings of the same silica nanoparticle content. The hardness of R05-5 coating markedly surpasses that of the R0-5 coating, which could result from the improved interfacial strength between polysiloxane and silica nanoparticles. Interesting mechanical results are revealed in the R10-X coating series. Compared with R0 coatings, the R10-5 coating has the same hardness, but better flexibility, and on the contrary, the R10-15 and R10-20 coatings have the same flexibility, but higher hardness. The R10-10 coating exhibits simultaneous enhancements in both hardness (7H) and flexibility (5 mm). This mechanical improvement is very desirable, and to our knowledge, never reported before. For the R28-X coating series, no ideal mechanical improvement was exhibited despite the high silica nanoparticle content. The above mechanical properties suggest that the moisture-curable polysiloxane coatings can be strengthened by MPS-modified silica nanoparticles. However, the mechanical enhancement strongly depends on the molar ratio of MPS to SiO_2.

The influence of MPS-to-SiO_2 molar ratio on the mechanical improvement may be interpreted by two effects imparted by MPS. MPS exists in two states in the wet coatings, free MPS and MPS that is bonded to silica nanoparticles. The MPS can establish chemical bonds with APS via aza-Michael reactions, but not all MPS can react with APS due to relatively fast moisture curing. The unreacted MPS then acts as a plasticizer in the dried coatings. MPS moieties that have reacted on the silica nanoparticles facilitate strong interactions between the polysiloxane matrix and silica nanoparticles. At low MPS-to-SiO_2 molar ratio, the quantity of MPS attached to silica nanoparticles is too small to promote strong interfacial interactions. Conversely, at high MPS-to-SiO_2 molar ratios, the polysiloxane matrix is less rigid due to plasticization by free MPS, which restricts reinforcement by the silica nanoparticles. The optimal molar ratio of MPS to SiO_2 was found to be 0.1:1.

The effect of APS dosage on the macro-mechanical properties of silicon-oxo coatings was also examined, and the results are tabulated in Table 2. The coatings with 10% and 20% APS (samples R10-10-10% and R10-10-20%) were soft and flexible. The low values of hardness suggest a low degree of crosslinking at low APS concentrations. Even at 50% APS dosage, high values of hardness were not achieved (R10-10-50%). The R10-10 coating (30% APS) still possesses the best mechanical performance. The lower hardness of R10-10-50% relative to R10-10 is due to the formation of aggregates via the fast hydrolysis/condensation of APS in air.[17] These aggregates were evidenced by the reduced transparency of the R10-10-50% coating. Therefore, appropriate APS dosage is critical for fabricating silicon-oxo-dominated nanocomposite coatings with optimized mechanical properties.

Micromechanical properties of silicon-oxo coatings

Nanoindentation tests are useful for evaluating the micromechanical properties of coatings. Therefore, such tests were conducted on the silicon-oxo composite coatings. Figure 3 displays the load-hold-unload curves of silicon-oxo-dominated coatings prepared with MPS-modified silica alcosol. Samples fabricated with unmodified silica alcosol are shown for comparison. As the load is increased, the penetration depth increases. Creep behavior is observed in all samples at the holding stage. Interestingly, all samples (except R0-5 and R05-10) almost completely recover when the load is released, regardless of the nanoparticle content or functionality, indicating that the silicon-oxo-dominated nanocomposite coatings have high elasticity that is similar to the moisture-curable polysiloxane coating (R0).

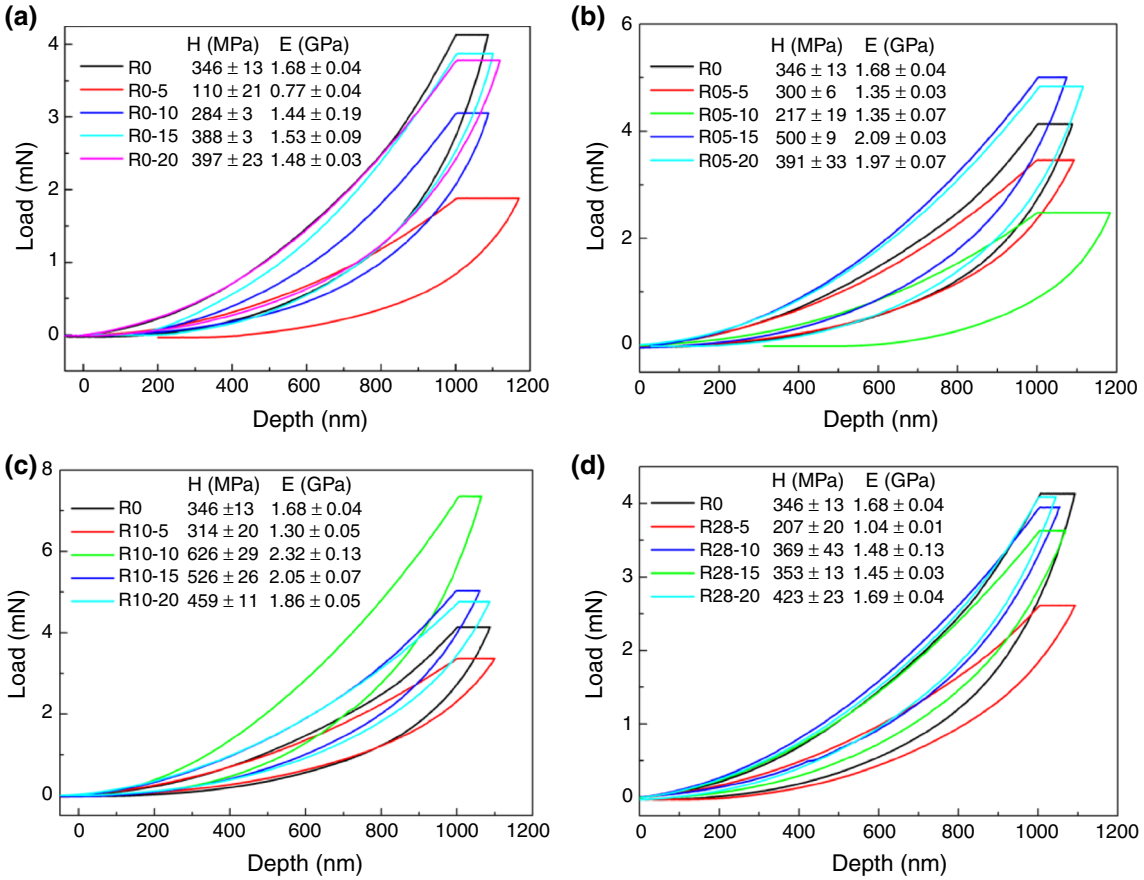

Fig. 3: The load-hold-unload curves of silicon-oxo-dominated nanocomposite coatings prepared with various molar ratios of MPS to SiO_2 nanoparticles: (a) unmodified; (b) 0.05:1; (c) 0.1:1; (d) 0.28:1

Microhardness (H) and elastic modulus (E) were derived from nanoindentation tests, and are also shown in Fig. 3. Figure 3a shows a significant reduction in microhardness after 5% of unmodified silica nanoparticles were added to the polysiloxane coating. Thereafter, the microhardness of the nanocomposite coatings gradually increases with increasing silica content. However, even at silica contents up to 20 wt%, its microhardness was only comparable to that of R0 coating. The elastic modulus shows a similar trend to the microhardness. The data agree with the macro-mechanical properties shown in Table 2. It further suggests that unmodified silica nanoparticles are not good candidates for reinforcing moisture-curable polysiloxane coatings.

Figures 3b–d show that the micromechanical properties of coatings embedded with modified silica nanoparticles change in an irregular way as a function of silica content, and they strongly depend on the MPS-to-SiO_2 molar ratio. A monotonous increase of the micromechanical properties is revealed only for coatings with S28 silica alcosol. Compared with the R0 coating, decreased rigidity is observed for all nanocomposite coatings with 5 wt% silica content. Nevertheless, the reduced rigidity is less severe than when unmodified silica nanoparticles are used. For coating series with S05, S10, and S28 silica sol, maximum microhardness values of 500, 626, and 423 MPa were attained at silica contents of 15, 10, and 20 wt%, respectively. A microhardness value of 626 MPa is significantly higher than that of the original polysiloxane coating (346 MPa), further demonstrating the efficient reinforcement role of S10 silica sol. Furthermore, the micromechanical data illustrate that the rigidity of the nanocomposite coatings increases and then decreases as the MPS-to-SiO_2 molar ratio increases, in spite of silica content. The highest microhardness and elastic modulus were consistently attained at 0.1:1 MPS:SiO_2 molar ratio. This trend is in agreement with the macro-mechanical properties and could be explained by the two effects imparted by the MPS molecule, as mentioned above.

Figure 4 shows the load-hold-unload curves of silicon-oxo nanocomposite coatings prepared at different APS dosages. The microhardnesses and elastic moduli are also given in the figure. With the exception of the R10-10-10% coating, all coatings display nearly complete recovery after the release of the indentation load. The highest hardness and elastic modulus were acquired at an APS dosage of 30%. When the APS

dosage is increased to 50%, both the hardness and the elastic modulus decrease, and these data are in good agreement with the pencil hardness measurements.

Effect of the curing process on mechanical properties

As discussed above, a dual-curing mechanism exists in the silicon-oxo coatings via hydrolysis/condensation and aza-Michael addition. These two curing mechanisms compete and interfere with one another. Since the hydrolysis/condensation is more sensitive to moisture and aza-Michael reaction is strongly related to temperature, the mechanical properties of the R10-10 coating are expected to be further optimized by changing the curing process. Therefore, two curing processes were designed as follows: (A) ambient curing for 1 day with subsequent heat treatment for 0.5 h at 100, 150, 170, 185, and 200°C; and (B) ambient curing for 7 days with subsequent heat treatment for 0.5 h at 100, 150, and 200°C.

Table 3 shows the macro-mechanical properties of the R10-10 coating dried under different conditions. As expected, the pencil hardness increases with increasing post-treatment temperature for both curing process, A and B. The extremely high pencil hardness of 9H (the highest grade pencil hardness) was reached at heat treatment temperatures of 185°C and 200°C in curing process A, and is superior to the highest pencil hardness (7H) achieved by curing process B. Nevertheless, a yellowing phenomenon was observed for sample A-200. This may be caused by the oxidization of amino groups that remain at relatively high concentrations in the coatings before post-treatment. In addition, Table 3 indicates that the flexibility deteriorates after post-treatment heating. However, sample A-185 still demonstrates equivalent flexibility as that of the R0 coating while demonstrating the highest pencil hardness (see Table 2). Therefore, hard (9H) and tough (flexibility = 10 mm) silicon-oxo nanocomposite coatings can be fabricated using an appropriate curing process.

The micromechanical properties of silicon-oxo coatings dried by different curing processes were also analyzed by nanoindentation tests. Figure 5 presents the load-hold-unload curves of typical samples A-185 and B-200. Both display excellent recovery of deformation, implying that the heat-induced hardness enhancement does not sacrifice elasticity in silicon-oxo

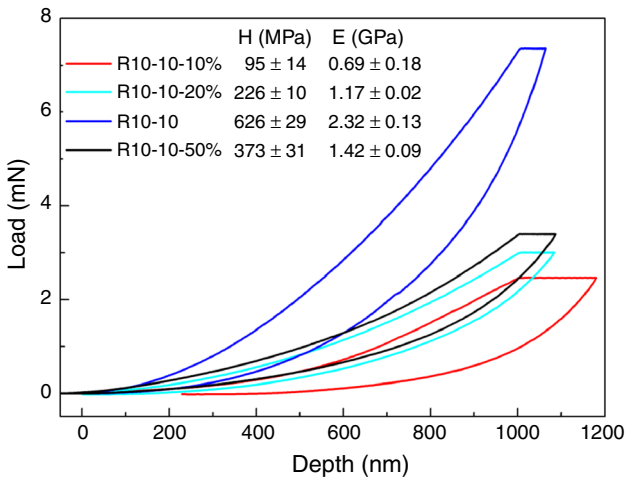

Fig. 4: The load-hold-unload curves of silicon-oxo nanocomposite coatings with different APS dosages

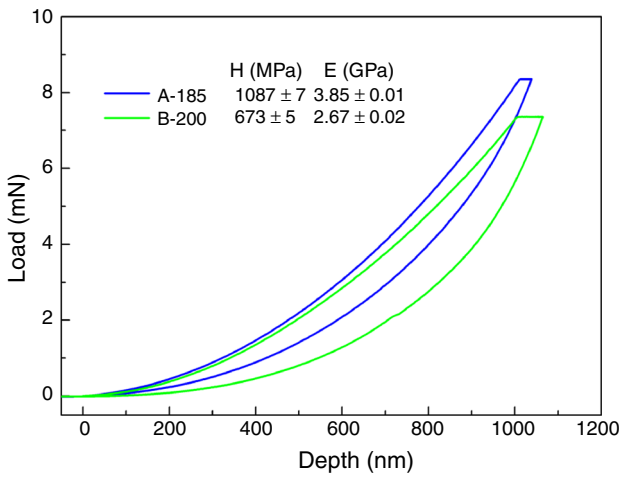

Fig. 5: The load-hold-unload curves of coatings A-185 and B-200

Table 3: Macro-mechanical properties of the R10-10 coating dried with different curing processes

Run	Curing process	Post-treatment temperature (°C)	Thickness (μm)	Pencil hardness	Flexibility (mm)	Appearance of dried coatings
A-100	A	100	13.8	3H	5	Colorless, clear
A-150	A	150	14.8	4H	5	Colorless, clear
A-170	A	170	14.8	6H	5	Colorless, clear
A-185	A	185	15.7	9H	10	Colorless, clear
A-200	A	200	13.7	9H	15	Yellowing
B-100	B	100	13.9	4H	5	Colorless, clear
B-150	B	150	16.0	5H	10	Colorless, clear
B-200	B	200	14.6	7H	10	Colorless, clear

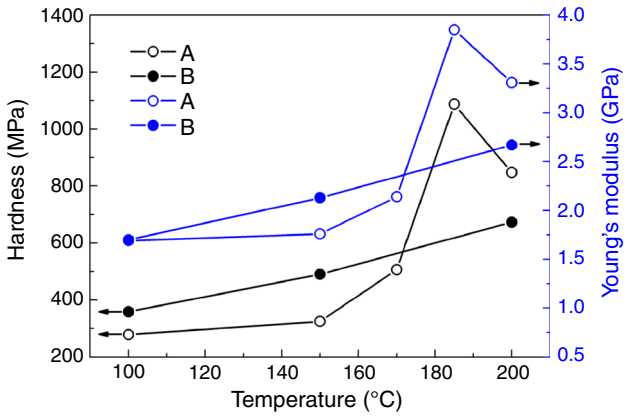

Fig. 6: The microhardness and Young's modulus of silicon-oxo coatings as a function of post-treatment temperature

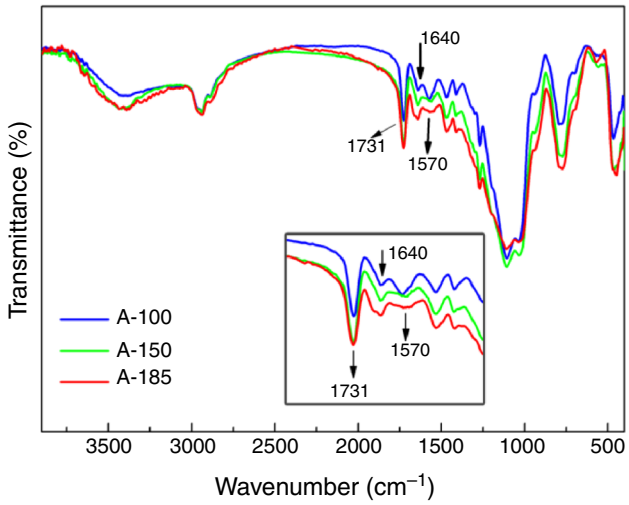

Fig. 7: FTIR spectra of A-100, A-150, and A-185 coatings

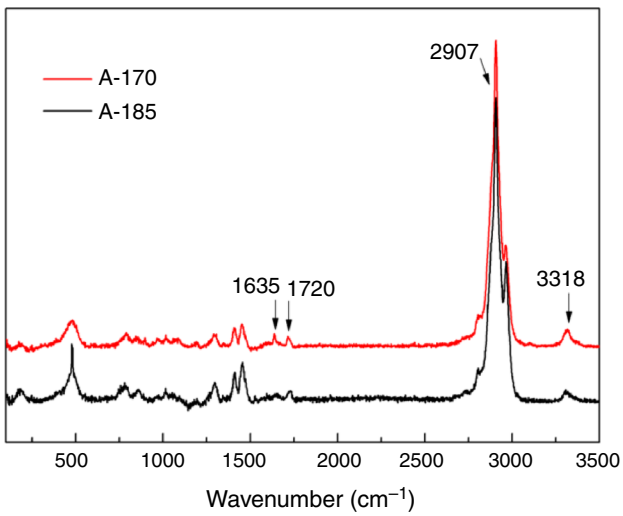

Fig. 8: Raman spectra of A-170 and A-185 coatings

coatings. The microhardness and Young's modulus of the silicon-oxo coatings as a function of post-treatment temperature are plotted in Fig. 6. For coatings dried with curing process A, the microhardness and Young's modulus are relatively constant at temperatures below 150°C and begin to increase at 170°C. The microhardness increased significantly to 1087 MPa at 185°C. This value exceeds the hardness (1.0 GPa[18]) of a dense sol–gel silica film. Because of oxidization, the microhardness and Young's modulus decline at 200°C. For samples dried by curing process B, both the microhardness and Young's modulus steadily increase with increasing temperature. Interestingly, the coatings at 100 and 150°C have higher hardnesses and Young's moduli than those correspondingly obtained by curing process A. However, the coating at 200°C exhibits inferior mechanical properties compared to the coatings at 185 and 200°C with curing process A. These micromechanical properties are consistent with the macro-mechanical properties as shown in Table 3, further suggesting that curing process A with post-treatment at 185°C is appropriate for obtaining coatings with high hardness.

FTIR and Raman spectroscopy were employed to better understand the mechanical properties of the A-185 coating. Figure 7 shows the FTIR spectra of the A-100, A-150, and A-185 coatings. The peaks at 1731 and 1640 cm^{-1} correspond to the stretching vibrations of C=O and C=C,[19] and the peak at 1570 cm^{-1} is assigned to the bending vibration of $-NH_2$. Because absorbed water can interfere with the peak at 1640 cm^{-1}, its intensity does not show a distinctive change as temperature is varied. Nevertheless, the intensity of the $-NH_2$ peak weakens as post-treatment temperature increases, signaling the occurrence of the aza-Michael reaction. Figure 8 presents the Raman spectra of A-170 and A-185. The peaks at 1635, 1720, 2907, and 3318 cm^{-1} represent the stretching vibrations of C=C, C=O, C–H, and N–H, respectively. A-185 has lower C=C and N–H peak intensities in comparison with A-170. If the peak at 2907 cm^{-1} is used as a reference, the area ratios of A_{1635}/A_{2907} and A_{3307}/A_{2907} are calculated to be 0.16 and 0.23 for A-170, and 0.02 and 0.04 for A-185, respectively. These results verify the existence of the aza-Michael reaction. Thus, the aza-Michael reaction at 185°C contributes to the excellent mechanical properties of A-185.

The aza-Michael reaction can actually occur at lower temperatures.[20] However, it is easily hindered by moisture curing that causes fast transformation of wet coatings into a solid state. Nevertheless, the aza-Michael reaction can resume at high temperatures. Considering the change in mechanical properties as a function of temperature, 150°C seems to be the critical temperature for restarting the aza-Michael reaction in coatings dried by curing process A. Since the degree of hydrolysis/condensation is higher for coatings dried by

curing process B, restarting the aza-Michael reaction is more difficult. Therefore, remarkable increases in hardness were not observed even if the post-treatment temperature was increased to 200°C.

The effect of heat treatment temperature on the scratch resistance of silicon-oxo coatings was evaluated by nanoscratch testing under a maximum load of 30 mN. Figure 9 shows the penetration depth profiles and the residual depth profiles of samples fabricated by curing process A. The penetration depth is shallower at high heating temperatures. This result is in agreement with the hardness measurements. The residual depth is much shallower than the penetration depth for all samples, indicating good reflow capability of the coatings, especially at penetration depths less than 685 nm. Fluctuations in the residual profiles at high load arise from cracks. These cracks can be observed in the photographs shown in Fig. 10. Upon careful inspection, cracks are found to occur at loads of 13, 17, and 25 mN for A150, A170, and A185, respectively. Additionally, the residual depth at a normal load of 5 mN was employed to evaluate the scratch resistance.[21] Good scratch resistance results when critical load values are high and residual indentation depths are low. Herein, the residual depths at 5 mN are 123, 130, and 92 nm for A-150, A-170, and A-185, respectively. Therefore, both the critical load and residual depth suggest that A185 demonstrates the best scratch resistance.

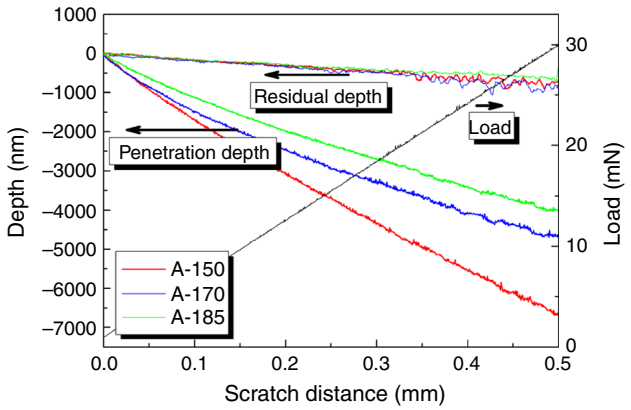

Fig. 9: Penetration depth and residual depth profiles of A-150, A-170, and A-185 coatings in nanoscratch tests

Conclusion

Thick silicon-oxo-dominated nanocomposite coatings were prepared from a moisture-curable polysiloxane oligomer, MPS-modified silica alcosol, and a curing agent, APS. It was found that modification of silica alcosol with MPS was necessary to attain high transparency coatings. The mechanical properties of the coatings strongly depend on the molar ratio of MPS to SiO_2 nanoparticles, silica nanoparticle content, and APS dosage. A hard (pencil hardness = 7H, and microhardness = 626 MPa) and tough (flexibility = 5 mm) coating was obtained after ambient curing for 1 week, followed by drying at 60°C overnight using the following formulation: MPS-to-SiO_2 molar ratio of 0.1:1, silica nanoparticle content of 10 wt%, and APS dosage of 30 wt%. By optimizing the curing process, a superhard (pencil hardness = 9H, and microhardness = 1087 MPa) and tough (flexibility = 10 mm) coating was achieved by 1 day of ambient drying followed by 0.5 h post-treatment at 185°C. Besides the condensation of Si-OR/Si-OH, remarkable mechanical property enhancements by optimizing the curing process were attributed to the aza-Michael reaction between C=C and $–NH_2$. Based on their prominent mechanical properties, silicon-oxo-dominated nanocomposite coatings show promise as scratch-resistant coatings for plastic, metal, wood, and other materials.

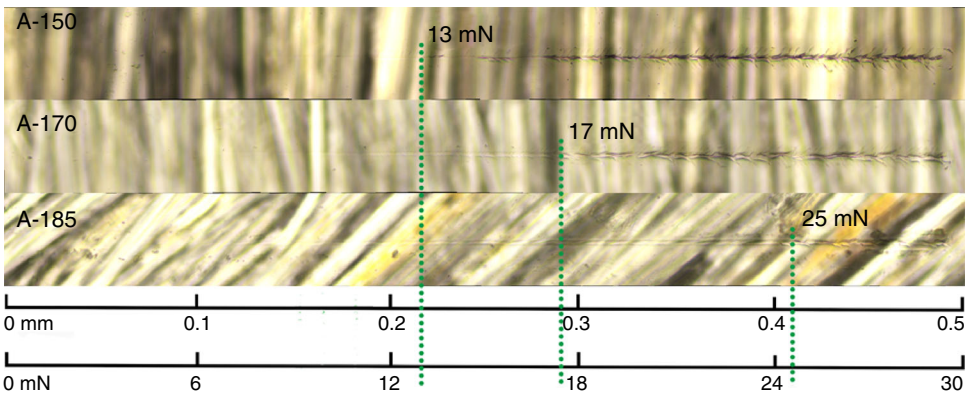

Fig. 10: A surface photograph of A-150, A-170, and A-185 coatings after nanoscratch tests

References

1. Nemeth, S, Liu, YC, ''Mechanical Properties of Hybrid Sol-Gel Derived Films as a Function of Composition and Thermal Treatment.'' *Thin Solid Films*, **517** 4888 (2009)
2. Conde, A, Durán, A, Damborenea, JJ De, ''Polymeric Sol-Gel Coatings as Protective Layers of Aluminium Alloys.'' *Prog. Org. Coat.*, **46** 288 (2003)
3. Que, WX, Zhang, QY, Chan, YC, Kam, CH, ''Sol-Gel Derived Hard Optical Coatings via Organic/Inorganic Composites.'' *Compos. Sci. Technol.*, **63** 347 (2003)
4. Kasten, LS, Balbyshev, VN, Donley, MS, ''Surface Analytical Study of Self-Assembled Nanophase Particle (SNAP) Surface Treatments.'' *Prog. Org. Coat.*, **47** 214 (2003)
5. Sarmento, VHV, Schiavetto, MG, Hammer, P, Benedetti, AV, Fugivara, CS, Suegama, PH, Pulcinelli, SH, Santilli, CV, ''Corrosion Protection of Stainless Steel by Polysiloxane Hybrid Coatings Prepared Using the Sol-Gel Process.'' *Surf. Coat. Technol.*, **204** 2689 (2010)
6. Fallet, M, Mahdjoub, H, Gautier, B, Bauer, JP, ''Electrochemical Behaviour of Ceramic Sol-Gel Coatings on Mild Steel.'' *J. Non-Cryst. Solids*, **293** 527 (2001)
7. Schmidt, H, ''New Type of Non-Crystalline Solids Between Inorganic and Organic Materials.'' *J. Non-Cryst. Solids*, **73** 681 (1985)
8. Mackenzie, JD, Bescher, EP, ''Physical Properties of Sol-Gel Coatings.'' *J. Sol-gel Sci. Technol.*, **19** 23 (2000)
9. Chen, XB, Zhou, SX, You, B, Wu, LM, ''Ambient-Curable Polysiloxane Coatings: Structure and Mechanical Properties.'' *J. Sol-gel Sci. Technol.*, **58** 490 (2011)
10. Chen, XB, Zhou, SX, You, B, Wu, LM, ''Mechanical Properties and Thermal Stability of Ambient-Cured Thick Polysiloxane Coatings Prepared by a Sol-Gel Process of Organoalkoxysilanes.'' *Prog. Org. Coat.*, **74** 540 (2012)
11. Mallakpour, S, Madani, M, ''The Effect of the Coupling Agents KH550 and KH570 on the Nanostructure and Interfacial Interaction of Zinc Oxide/Chiral Poly(Amide-Imide) Nanocomposites Containing L-Leucine Amino Acid Moieties.'' *J. Mater. Sci.*, **49** 5112 (2014)
12. Na, M, Park, H, Kang, D, Ahn, M, Lee, H, ''Characteristics of Nanohybrid Coating Films Synthesized from Colloidal Silica and Organoalkoxysilanes by Sol-Gel Process.'' *Jpn. Appl. Phys.*, **47** 538 (2008)
13. Abdollahi, H, Ershad-Langroudi, A, Salimi, A, Rahimi, A, ''Anticorrosive Coatings Prepared Using Epoxy-Silica Hybrid Nanocomposite Materials.'' *Ind. Eng. Chem. Res.*, **53** 10858 (2014)
14. Lu, YF, Zhou, SX, Gu, GX, Wu, LM, ''Preparation of Transparent, Hard Thermochromic Polysiloxane/Tungsten-Doped Vanadium Dioxide Nanocomposite Coatings at Ambient Temperature.'' *Thin Solid Films*, **534** 231 (2013)
15. Oliver, WC, Pharr, GM, ''An Improved Technique for Determining Hardness and Elastic Modulus Using Load and Displacement Sensing Indentation Experiments.'' *J. Mater. Res.*, **7** 1564 (1992)
16. Chen, GD, Zhou, SX, Gu, GX, Wu, LM, ''Modification of Colloidal Silica on the Mechanical Properties of Acrylic Based Polyurethane/Silica Composites.'' *Colloids Surf. A Physicochem. Eng. Asp.*, **296** 29 (2007)
17. Phonthamachai, N, Chia, H, Li, X, Wang, F, Tjiu, WW, He, C, ''Solvent-Free One-Pot Synthesis of High Performance Silica/Epoxy Nanocomposites.'' *Polymer*, **51** 5377 (2010)
18. Sellinger, A, Weiss, PM, Nguyen, A, Lu, Y, Assink, RA, Gong, W, Brinker, CJ, ''Continuous Self-Assembly of Organic-Inorganic Nanocomposite Coatings That Mimic Nacre.'' *Nature*, **394** 256 (1998)
19. Lin, JB, Chen, HL, Ji, Y, Zhang, Y, ''Functionally Modified Monodisperse Core-Shell Silica Nanoparticles: Silane Coupling Agent as Capping and Size Tuning Agent.'' *Colloids Surf. A Physicochem. Eng. Asp.*, **411** 111 (2012)
20. Mather, BD, Viswanathan, K, Miller, KM, Long, TE, ''Michael Addition Reactions in Macromolecular Design for Emerging Technologies.'' *Prog. Polym. Sci.*, **31** 487 (2006)
21. Osterhold, M, Wagner, G, ''Methods for Characterizing the Mar Resistance.'' *Prog. Org. Coat.*, **45** 365 (2002)